Supporting Information for

Giant Valley Polarization in Janus 1T-*MNY* (*M*=Mo, W; *Y*=Br, Cl) monolayers: A New Class of Ferrovalley Materials

Ning Wang, Jianping Zhang, Weixin Liu, Xuanzheng Chen, Weixiao Ji, Changwen Zhang, Shishen Yan, Yaping Wang*, and Shengshi Li*

Spintronics Institute & School of Physics and Technology, University of Jinan, Jinan, Shandong, 250022, People's Republic of China.

Corresponding authors: sps_wangyp@ujn.edu.cn (Y. Wang); sdy_liss@ujn.edu.cn (S. Li)

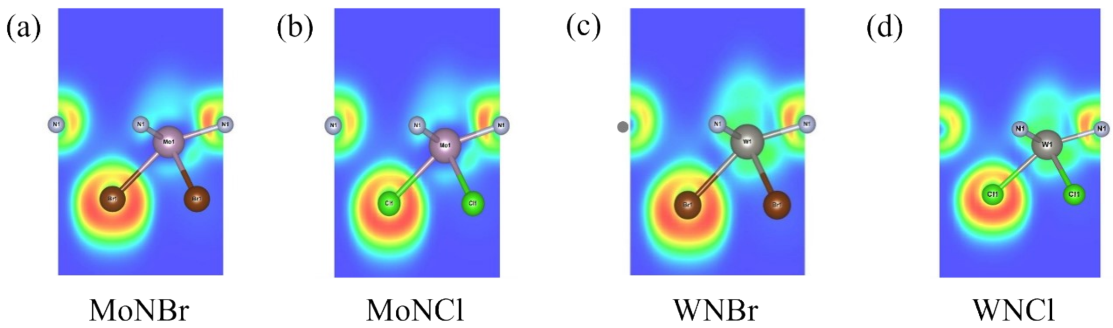

Fig. S1. Electron localization function of MoNBr, MoNCl, WNBr, and WNCl monolayers.

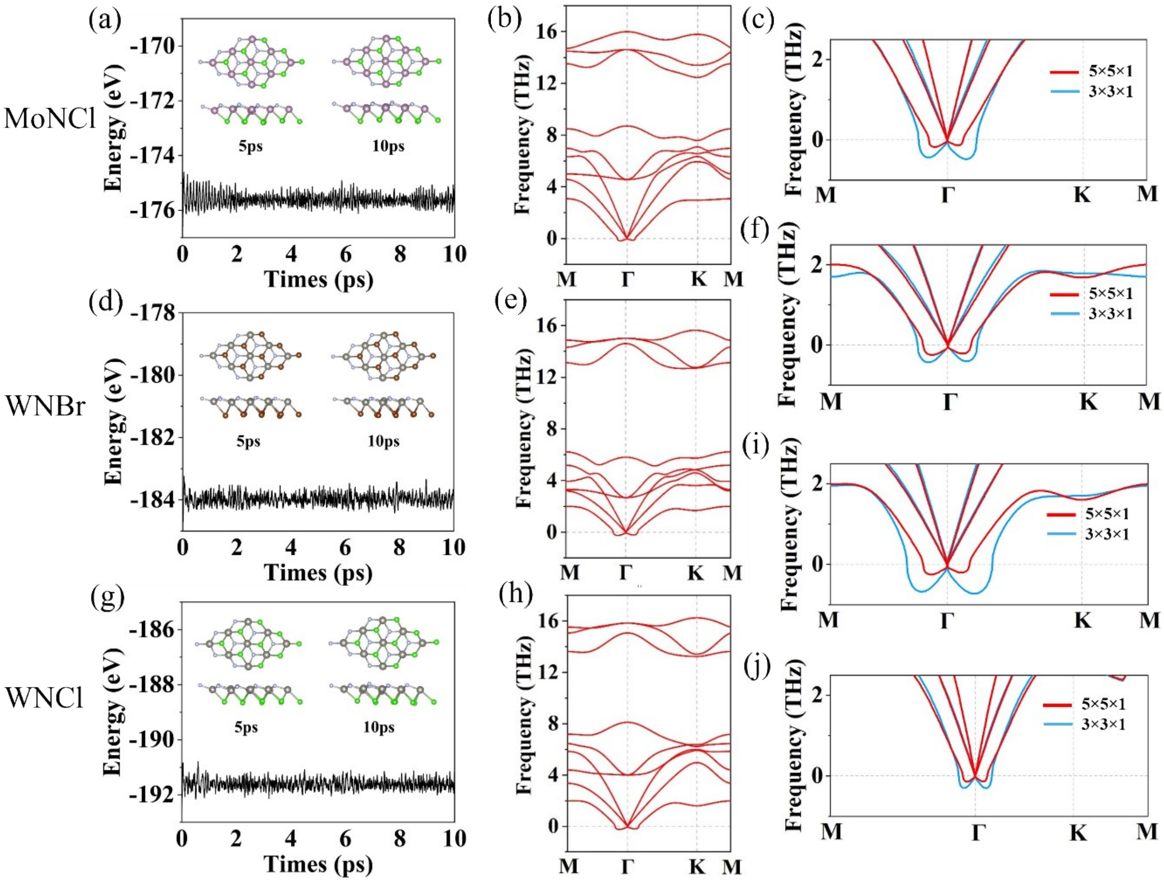

Fig. S2. The total energy evolution over time, phonon spectrum, and magnified views of the acoustic branches calculated at different supercell sizes for the MoNCl (a-c), WNBr (d-f), and WNCl (g-i) monolayers. The insets in (a), (d), and (g) are structural snapshots of MoNCl, WNBr, and WNCl monolayers at 5ps and 10 ps. (j) Magnified views of the acoustic branches calculated at different supercell sizes for the MoNBr monolayer.

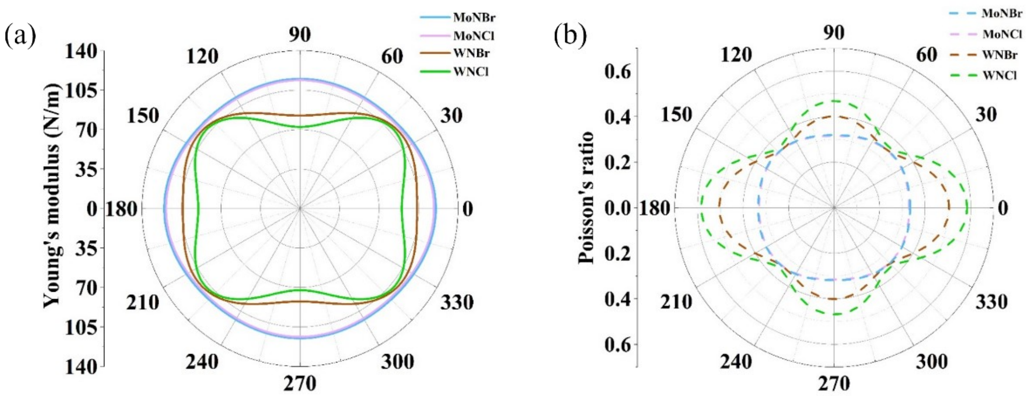

Fig. S3. (a) Young's modulus and (b) Poisson's ratio of *M*N*Y* monolayers.

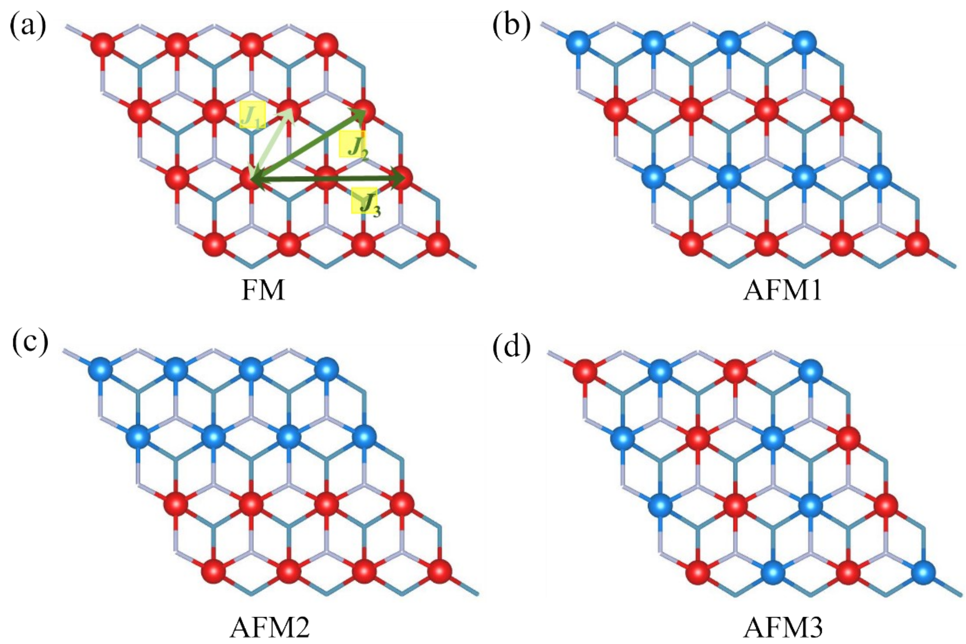

Fig. S4. Top view of ferromagnetic (a) and antiferromagnetic (b-d) configuration for MNY monolayers. J_1, J_2 and J_3 in the (a) represent the nearest-neighbor exchange coupling parameter.

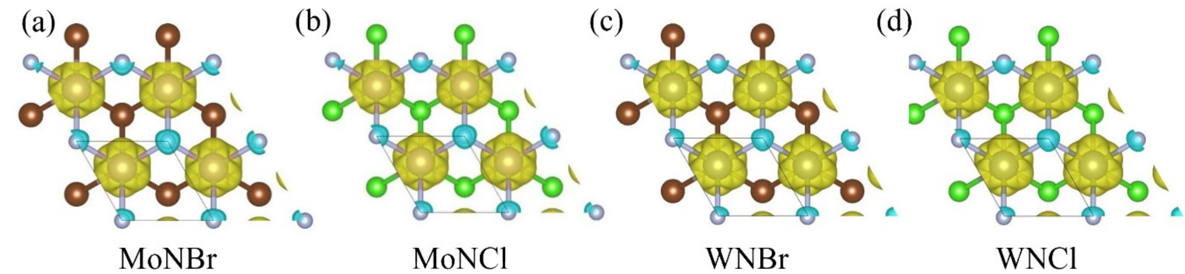

Fig. S5. Spin density distribution of MoNBr, MoNCl, WNBr, and WNCl monolayers.

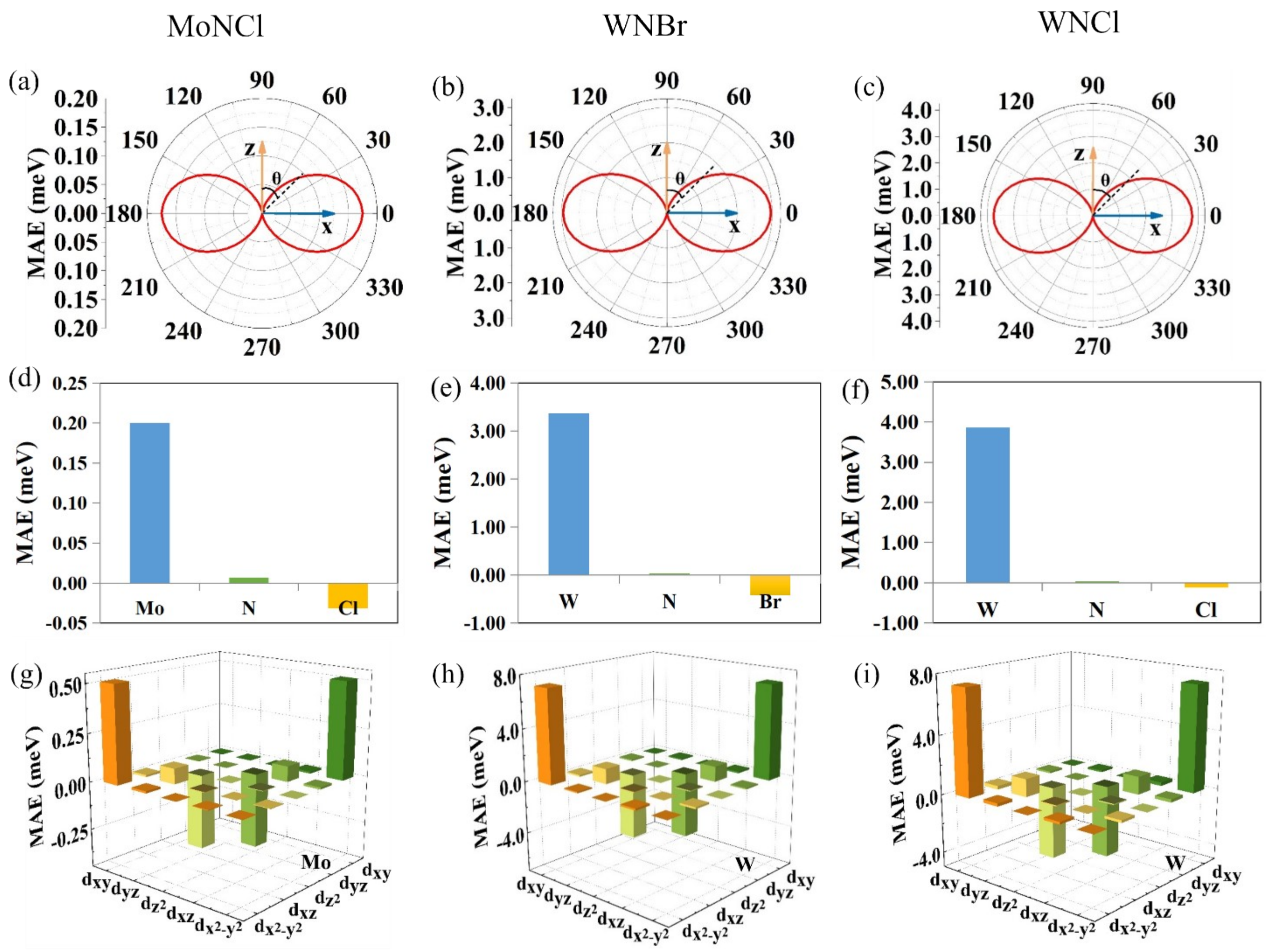

Fig. S6. Angular dependence of MAE (a-c), atom-resolved MAE (d-f) and orbital-resolved MAE (g-i) for the MoNCl, WNBr, and WNCl monolayers.

Table S1. Nearest-neighbor (J_1), next-nearest-neighbor (J_2), and third-nearest-neighbor (J_3) exchange coupling parameters of *M*N*Y* monolayers.

	MoNBr	MoNCl	WNBr	WNCl
J_1(meV)	50.26	60.22	21.27	21.33
J_2(meV)	-23.17	-32.98	-0.69	-0.72
J_3(meV)	12.3	17.42	0.72	0.86

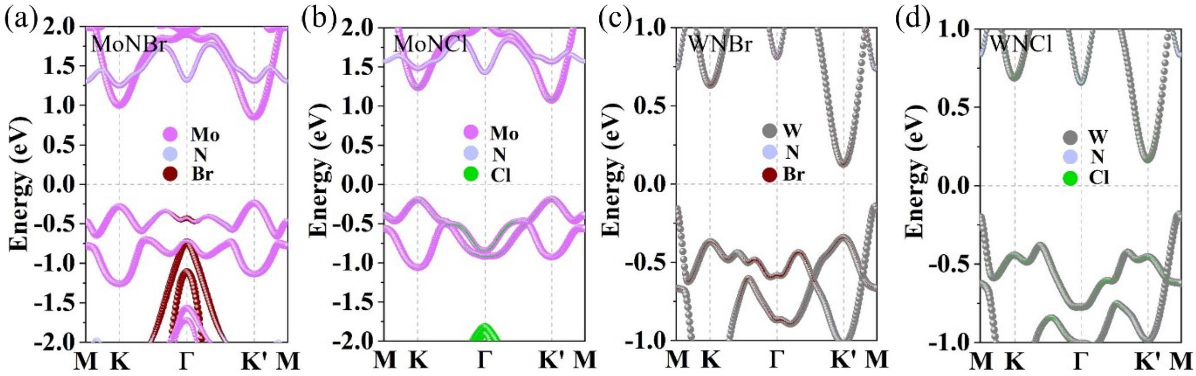

Fig. S7. Atom-resolved band structures of MoNBr, MoNCl, WNBr, and WNCl monolayers.

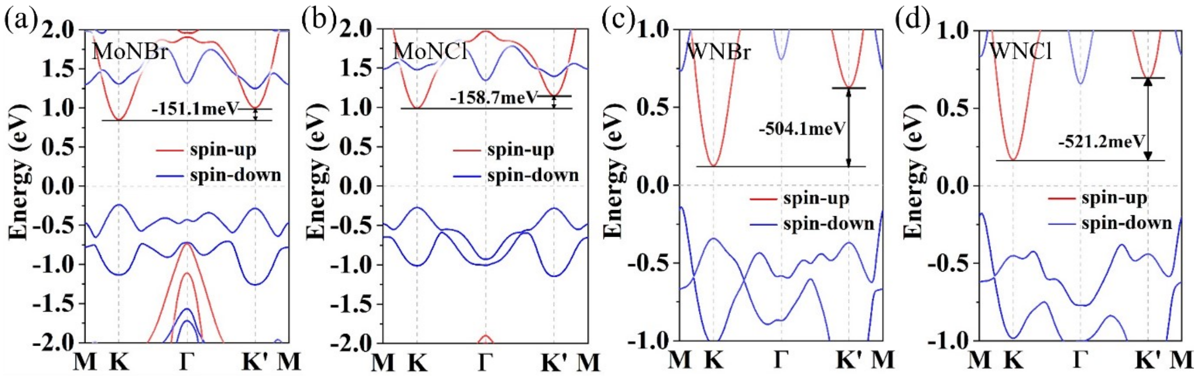

Fig. S8. Calculated SOC band structures of MoNBr, MoNCl, WNBr, and WNCl monolayers with downward magnetization.

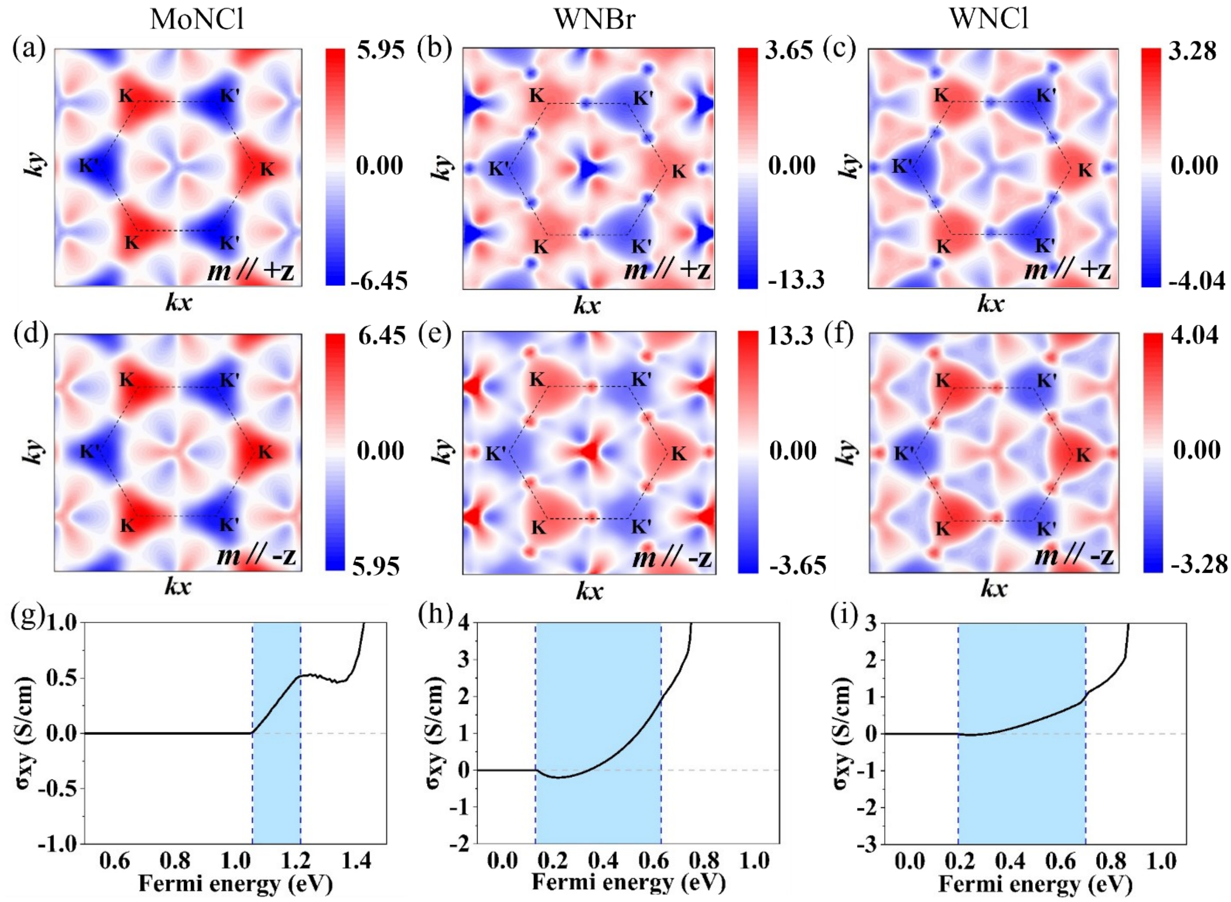

Fig. S9. The Berry curvature distributions in the Brillouin zone of MoNCl (a, d), WNBr (b, e), and WNCl (c, f) monolayers with magnetization along +z and −z directions. (g-h) Calculated anomalous Hall conductivity σ_{xy} as a function of Fermi energy for MoNCl, WNBr, and WNCl monolayers.

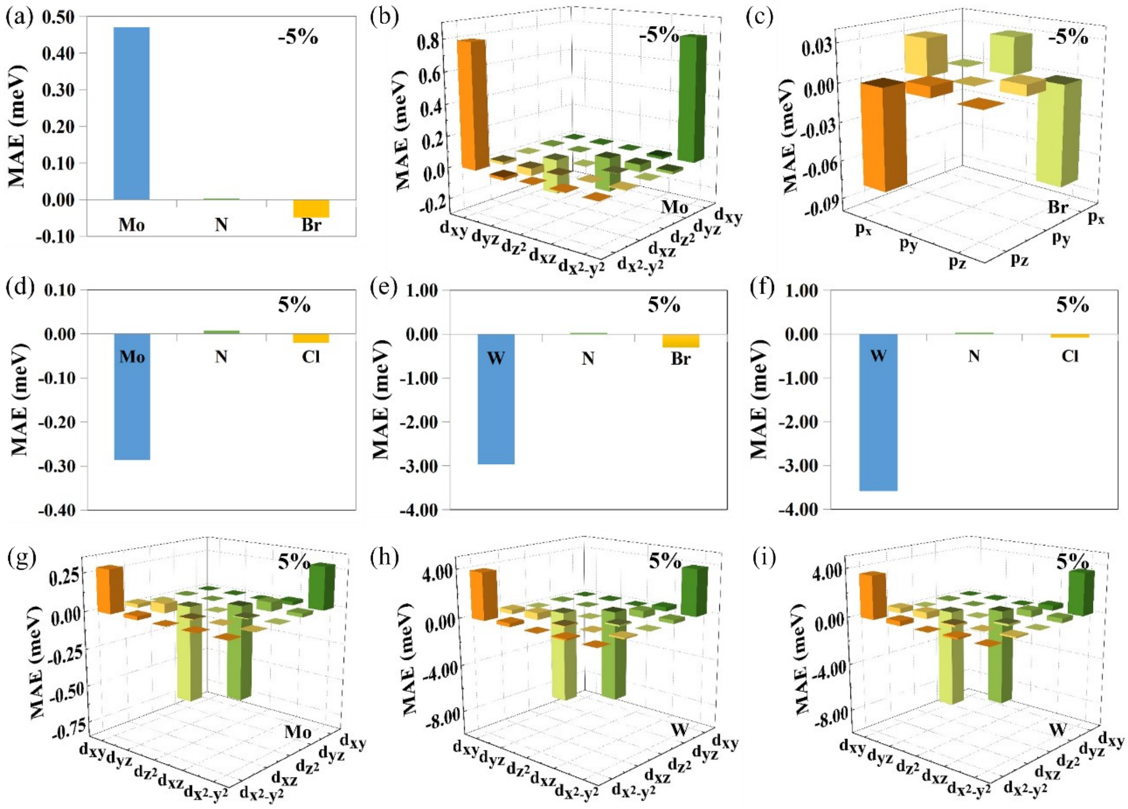

Fig. S10. (a-c) Atom- and orbital-resolved MAE of the MoNBr monolayer under 5% compressive strain. (d-i) Atom- and orbital-resolved MAE for the MoNCl, WNBr, and WNCl monolayers under 5% tensile strain.

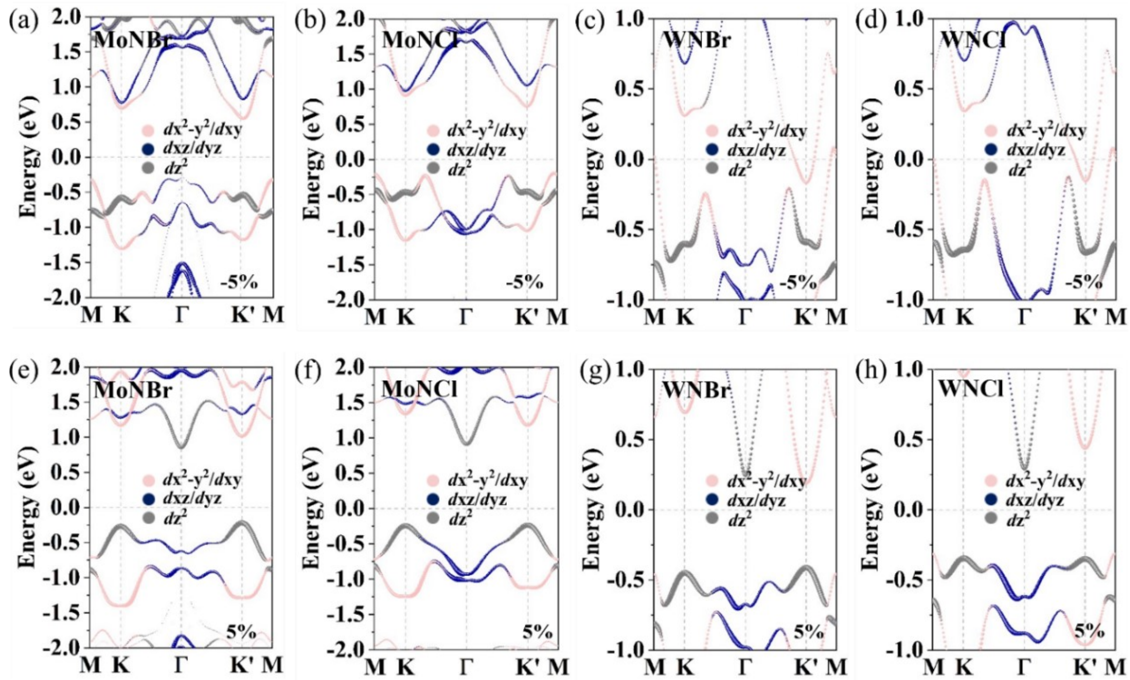

Fig. S11. Orbital-resolved SOC band structures of the MoNBr, MoNCl, WNBr, and WNCl monolayers under 5% compressive strain (a-d) and 5% tensile strain (e-h).

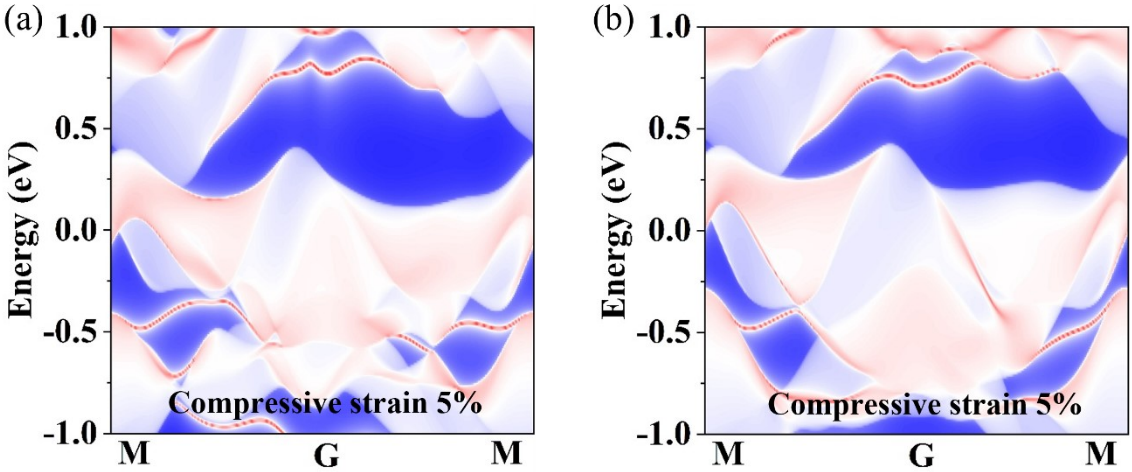

Fig. S12. Calculated edge states of WNBr (a) and WNCl (b) monolayers under 5% compressive strain.

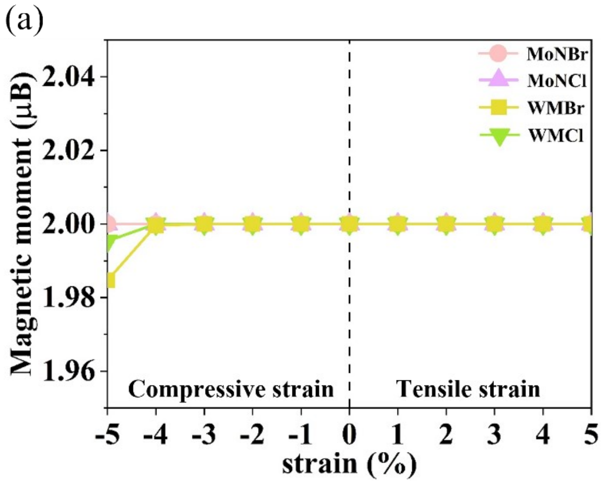

Fig. S13. Strain-dependent variation of the net magnetic moment of *M*N*Y* monolayers.

Table S2. Calculated piezoelectric stress coefficients e_{11} and e_{31} along with their respective ionic and electronic contributions.

	e_{11} (C/m)	e_{11}^{elc} (C/m)	e_{11}^{ion} (C/m)	e_{31} (C/m)	e_{31}^{elc} (C/m)	e_{31}^{ion} (C/m)
MoNBr	-1.03	-0.14	-0.89	0.09	0.03	0.06
MoNCl	-0.67	0.23	-0.90	0.41	0.40	0.01
WNBr	-0.33	0.23	-0.56	-0.34	-0.44	0.10
WNCl	-0.32	0.88	-1.20	-0.09	-0.12	0.03